30th Congress of the International Council of the Aeronautical Sciences
DCC, Daejeon, Korea ; September 25-30, 2016

AN EXPERIMENTAL AND COMPUTATIONAL STUDY OF THE AERODYNAMIC CHARACTERISTICS AN OSCILLATORY PITCHING NACA0012 AEROFOIL

Ashim Yadav, Simon Prince & Jenny Holt
School of Aerospace, Transport and Manufacturing, Cranfield University, UK.

Keywords: *Dynamically pitching aerofoil, Dynamic stall, Experiments, CFD.*

Abstract

The development and validation of a small scale oscillatory pitch and heave test rig, is documented, which was designed to enable the preliminary, comparative testing of flow control methods to manipulate the complex unsteady flows associated with pitching aerofoils, particularly involving dynamic stall.

The results of the initial commissioning tests, reported in this paper, have shown that the rig, and the associated measurement instrumentation, should be able to resolve the effect of flow control, if that effect is relatively large.

1 Introduction

This paper presents details of a small scale pilot wind tunnel facility which is being developed to allow comparative testing of flow control devices for the suppression of flow separations from dynamically pitching aerofoils. The aim is to provide a relatively cheap capability to quickly, but effectively, assess whether a given flow control methodology has realistic authority in controlling flow separations. Data from this facility can then inform the program for more accurate and detailed testing at much more representative scales in bigger facilities, and help reduce the overall time and cost of such developmental testing.

The experimental testing of flow control methods will also be supported via focused computational simulation, through which it is hoped to shed light on the flow physics associated with separation and its suppression. This paper also presents the initial results from a study to identify suitable CFD methodologies which might be used to predict the complex unsteady flows associated with oscillatory pitching aerofoils.

An overview of the particular aerodynamic problem of dynamic stall, which is a focus for flow control development, is presented before the wind tunnel working section mechanism for the simulation of the pitching and heaving motion typical of a helicopter blade section is described. Comparisons between CFD and experimental data are then presented to demonstrate the capability of both the wind tunnel and CFD methodologies to predict the unsteady aerodynamic characteristics, to a level suitable for comparative studies of flow control devices.

2. Unsteady Aerodynamics of Dynamically Pitching Aerofoils

Studies of the aerodynamic characteristics of dynamically pitching aerofoils have been undertaken since at least the early 1920s [1-3]. It was soon discovered that the effect of viscosity led to the formation of “hysteresis loops” in lift and corresponding effects in the pitching moment and drag characteristics [4]. This phase lag in lift (circulation), whereby the lift is lower than the steady state value when α is increasing with time and higher than the steady state value when α is decreasing with time, as most notably modelled in 1935 by Theodorsen [5].

This situation is complicated by the effects of boundary later separation, and stall, when the peak angle of attack during the oscillation overshoots the static stall angle, and a process called "dynamic stall" then occurs. Fig 1 presents the typical lift and pitching moment (quarter chord) variation with angle of attack during oscillatory pitching of an aerofoil with dynamic stall. Here, the static lift and pitching moment behavior is depicted by the red-dashed lines, where no hysteresis effects are shown. In reality, some hysteresis effects can occur between upstroke and downstroke even with effectively zero pitching rate.

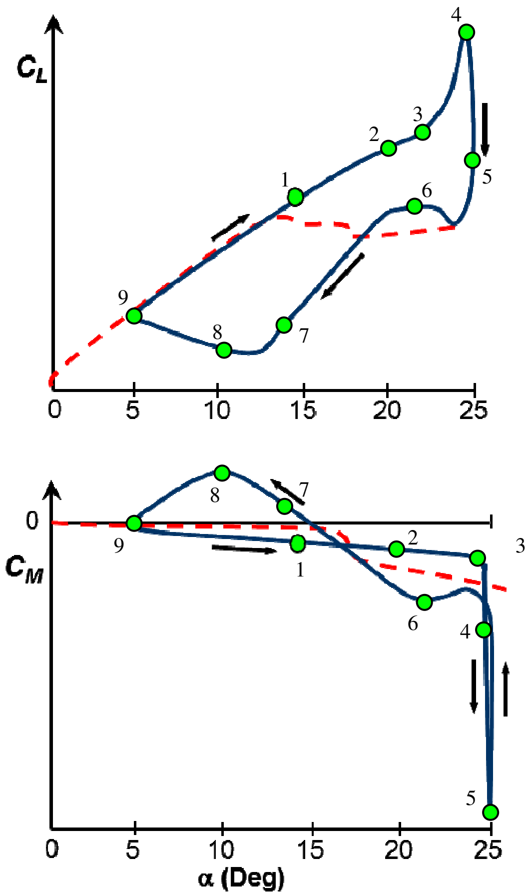

Fig 1: Dynamic stall events on a NACA0012 as determined at low Mach number (based on McAlister et al [6])

As the aerofoil α increases during the upstroke with an appreciable rate of pitching motion, the boundary layer on the upper surface will remain attached beyond the static stall angle of attack, with the trailing edge separation event delayed to much higher α, than occurs in static pitch conditions, as shown in figure 2. This corresponds with the continuation of the linear lift and pitching moment trend (point 1 in figure 1).

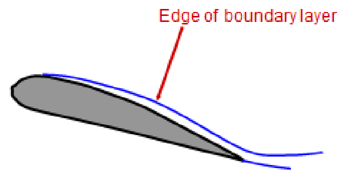

Fig 2: Depiction of the pre-stall flow state (condition 1 and 11 in fig. 1)

At some value of α, much higher than the static stall value, the static pressure levels will have risen on the upper surface to a point where the boundary layer will begin to separate from the trailing edge, as shown in figure 3, corresponding to point 2 in figure 1.

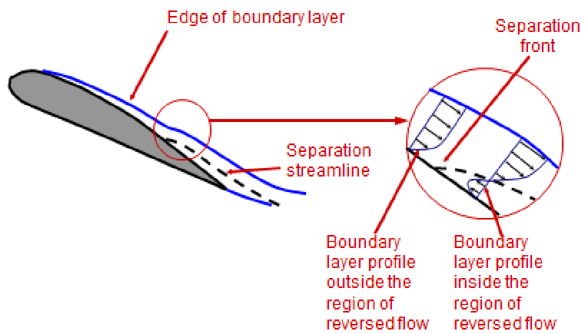

Fig 3: Depiction of the flow state following trailing edge separation during the upstroke (condition 2 in fig 1).

A further increase in α results in the rapid upstream propagation of the separation front until it reaches the vicinity of the leading edge, when a leading edge dynamic stall vortex (DSV) begins to form, as illustrated in figure 4. The suction from this vortex, acting on the aerofoil upper surface, results in a non-linear increase in the lift force, often leading to a sharp spike in the lift curve.

By this stage, the significantly enhanced leading edge suction levels give rise to a sharp increase in negative (nose-up) pitching moment, and a rapid pitching moment stall is initiated. The dynamic stall vortex then rapidly grows in size and strength, until the peak lift value is achieved (condition 4 in figure 1).

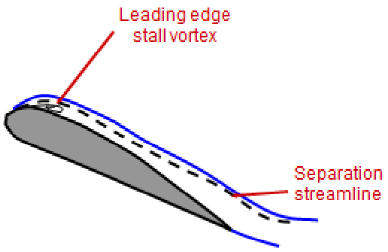

Fig 4: Depiction of the flow state with incipient leading edge stall vortex, upstroke (condition 3).

As the aerofoil passes beyond the peak of its pitching motion, the stall vortex will begin to convect downstream as shown in figure 5, an almost instantaneous lift stall will occur, and soon after the nose-up pitching moment will reach its peak value (condition 5 in figure 1).

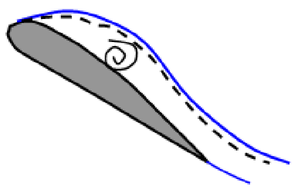

Fig 5: Depiction of the flow state at peak C_L, (condition 5 in figure 1).

During the down-stroke the passage of the stall vortex downstream to the trailing edge is a very rapid process and as it reaches the trailing edge, a weaker secondary vortex is sometimes formed from the trailing edge, as depicted in figure 6. This can cause a secondary inversion in the pitching moment curve and a levelling off of the lift level, corresponding to condition 6 in figure 1.

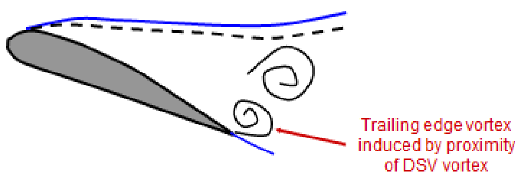

Fig 6: Depiction of the fully stalled flow state on the downstroke, with the formation of a trailing edge vortex (condition 6 in figure 1).

The flow then becomes fully stalled during much of the downstroke movement, with no attached flow on the upper surface (condition 6-7 in figure 1). At some point during the downstroke, as the lift continues to reduce and the pitching moment coefficient becomes more positive, the flow will re-attach to the leading edge of the aerofoil and leading edge suction will be re-established, as shown in figure 7. The separation front then moves back downstream, a maximum positive pitching moment will occur while the lift levels begin to rise again. Often the lift curve will return to its static pitching behavior around the start of the upstroke (condition 9 in figure 1), and the process begins again.

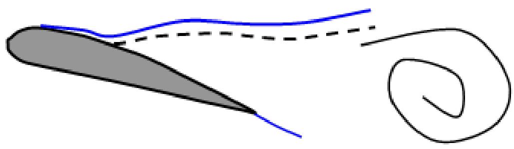

Fig 7: Depiction of the flow state post leading edge boundary layer attachment / suction recovery during pitch down (condition 8 in figure 1).

The occurrence of dynamic stall is generally detrimental. For instance, with its occurrence on a helicopter rotor blade, typically during the retreating portion of its rotation, the very high peak lift levels and negative pitching moments result in very high loads at the rotor hub, which result in vibration problems and seriously reduced component fatigue life issues.

There has therefore been much recent emphasis on the development of suitable flow control methods for the effective suppression of the formation of the DSV [7 -9]. The purpose of this paper is to report on the first results from the development of a small scale testing facility designed to assess, by comparative experimentation, the effectiveness of various flow control methods for this application.

3 The Small Scale Pitch and Heave Rig

A special working section, shown in figure 8, was designed at City University, London, for the testing of 2D aerofoils undergoing simple harmonic motion perpendicular to the airflow (heave) while simultaneously undergoing sinusoidal pitching motion. The rig was manufactured as part of a modular working section (0.54m x 0.50m section) for a low speed wind tunnel, now at Cranfield University.

Both heave and pitch motions are generated by rotating cam wheels, driven by an electric motor, which move push rods. The heave cam drives a push rod which is directly connected to the wind tunnel model axle shaft such that the up-down movement of the rod affects the heave motion of the model. This mechanism is independent of the pitch mechanism, which is driven be a separate cam wheel. Both the heave cam shaft and the pitch cam shaft are connected via a belt, and thereby rotate together.

The pitch cam drives a push rod which applies simple harmonic motion to pitch arm 1, which pivots from a fixed point on the heave push rod. The pitch push rod is located at the centre of pitch arm 1 and transfers its vertical movement to a second pitch arm which is connected, via an offset pitch lever, to the model axle. The movement of the pitch push rod thereby rotates the model axle in simple harmonic motion, independent of the heave mechanism.

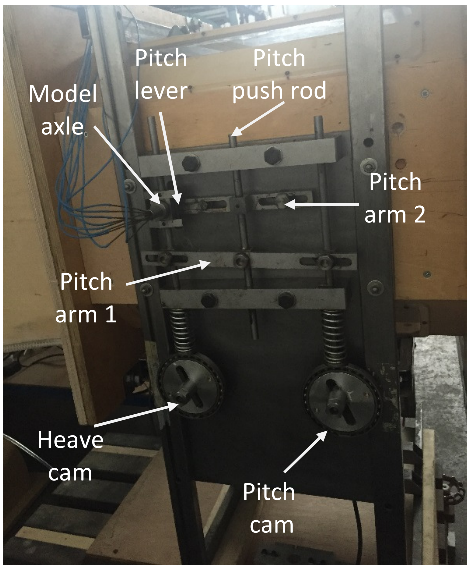

a) Left side of wind tunnel working section.

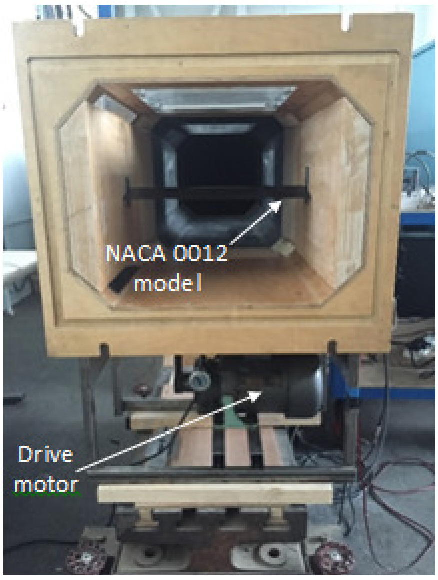

b) View inside the wind tunnel working section looking into the exit.

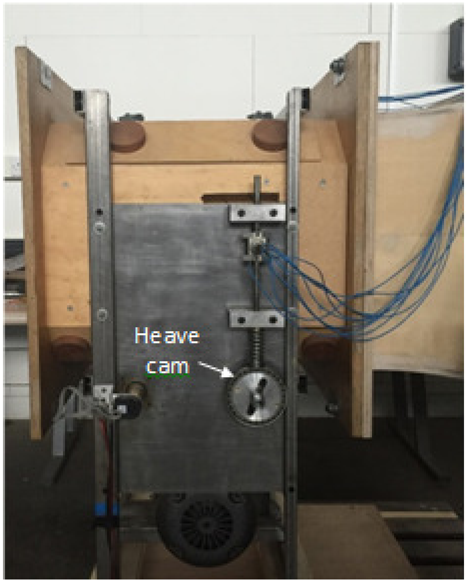

c) Right side of wind tunnel working section.

Fig 8: Details of the wind tunnel heave-pitch mechanism.

The heave motion is set by the offset between the heave cam wheel and the main drive shaft, while the sinusoidal pitching of the model, about its axle axis (the aerofoil quarter chord in this case) is set by the offset between the pitch cam and its drive shaft (which sets the cyclic motion), together with the setting of the pitch push rod (which fixes the collective pitch).

4 Experimental Testing

Once completed, the rig was instrumented and underwent a series of commissioning tests with a simple NACA0012 model.

Rotation of the pitch cam was measured using a potentiometer to an accuracy of ±0.05°. A calibration was performed between the potentiometer voltage, pitch cam rotation and model angle of attack, the measurement accuracy of which was estimated at ±0.25°. The 0.2kW single phase electric drive motor was capable of rotating the main drive shaft in the range 320-2880 rpm. The working section was connected to the Cranfield 0.5m x 0.54m open-return low speed wind tunnel. The model used for this initial study was a 0.54m span NACA0012 model of chord, c = 0.125m. Aerofoil surface pressure was measured via 19 centre-span pressure taps, with one located on the leading edge and another on the trailing edge. These were connected, via brass tubing, to 1000kHz Kulite dynamic differential pressure sensors, with an estimated accuracy of Cp = ±0.01 at the wind speed of U_∞ = 22m/s, which was maintained constant during the testing.

For these initial series of tests, the heave and collective pitch were set at zero so that only sinusoidal cyclic pitching motion was investigated. Tests were conducted for 5°, 10° and 15° of cyclic pitch at reduced pitching frequencies of $k = \omega c/2U_\infty$ = 0.1, 0.15, 0.23 and 0.33.

Measured surface pressure was acquired every 1 millisecond and corrected for both solid body and wake blockage effects [10], before the data was integrated, using a trapezium rule approach, to give lift coefficient, C_L, and drag coefficient, C_D. Data synchronization and processing was achieved through a bespoke LabView program which processed the tunnel dynamic pressure, cam rotation voltage and model surface pressures.

Figure 9 presents the typical variation of measured upper surface pressure distribution with angle of attack (on the upstroke in this case) obtained through this method for a chordwise Reynolds number, Re_c , of 1.48×10^5 (constant for all cases) and a pitching motion of $\alpha = 10^0 \sin\omega t$ and a reduced frequency of 0.1. It is expected that, despite the relatively low Reynolds number, the unsteady flow will be predominantly turbulent, rather than laminar, due the turbulence levels in the freestream flow, and the mechanical vibrations from the pitching.

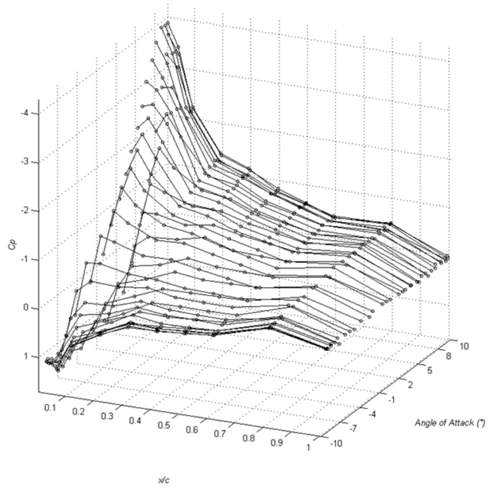

Fig 9: Variation of upper surface pressure with angle of attack for pitching NACA 0012 aerofoil, U=22m/s, $Re_c = 1.48\times10^5$, f = 5.6Hz, k=0.1, $\alpha = 10^0 \sin\omega t$.

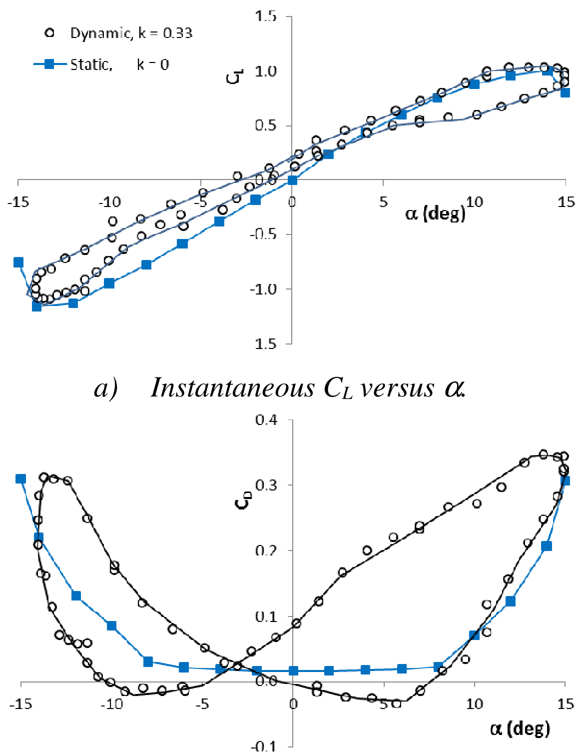

a) Instantaneous C_L versus α.

b) Instantaneous C_D versus α.

Fig 10: Variation of C_L and C_D with angle of attack for pitching NACA 0012 aerofoil, U=22m/s, $Re_c = 1.48\times10^5$, f = 5.6Hz, k=0.33, $\alpha = 15^0 \sin\omega t$.

Figure 10 compares the integrated forces for the cases of the statically pitched aerofoil model and the dynamically pitched model for a pitching motion of $\alpha = 15^0 \sin\omega t$ and a reduced frequency of 0.1.

5 Computational Modelling

In order to help validate the method, it was decided to compute the experimental flows using a time accurate Reynolds Averaged Navier-Stokes solver and a gridding and solution methodology that has been shown to provide good comparative data in previous studies [11-12].

The FLUENT commercial CFD solver was employed and was first used to compute two cases, in purely 2D, from the classic experimental dynamic stall study of McAlister et al [6]. A dynamic mesh method, using a baseline multi-block structured O-grid with the first cell height from the wall set to $1\text{x}10^{-5}c$ was employed. Specifically, the spring-based smoothing method was employed. The grid comprised an inner structured O-type grid, fixed to the aerofoil with a circular outer boundary interface, surrounded by an unstructured outer grid, with the farfield boundary fixed, a distance of ~50 chord lengths away. Sinusoidal motion was applied to the inner grid, set through the User Defined Functions facility.

The pressure based transient solver was employed with the SIMPLE pressure-velocity coupling algorithm. Two turbulent boundary layer cases were chosen for simulation, and the Spalart-Allmaras (S-A) and k-ω SST turbulence models were tested. A time step of 1 millisecond was used with a maximum of 50 iterations per time-step and the convergence criteria set to 10^{-5}.

The two cases chosen for simulation were for a freestream Mach number of 0.09, with Re_c=2.5x10^6, and a pitching motion with 15° of collective pitch and a 10° sinusoidal cyclic pitch. The first case was for a pitching frequency of 0.41Hz (k = 0.05) and the second for a pitching frequency of 1.22Hz (k = 0.15).

Figure 11 presents the comparison between the measured variations of the aerodynamic characteristics with angle of attack with the CFD predicted data for the case of k = 0.05.

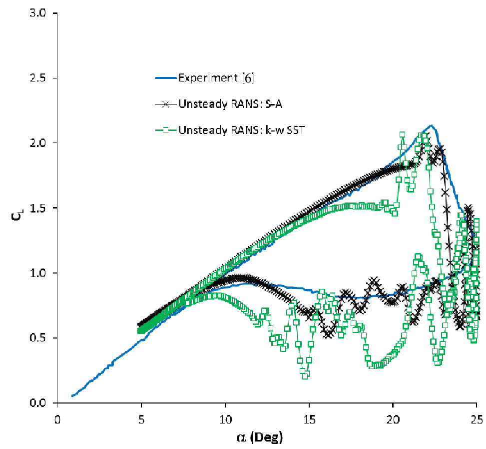

a) C_L versus α.

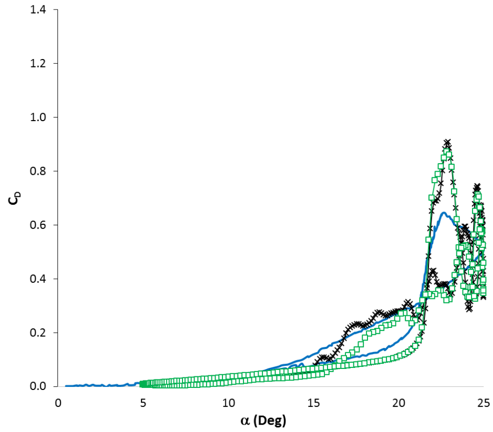

b) C_D versus α.

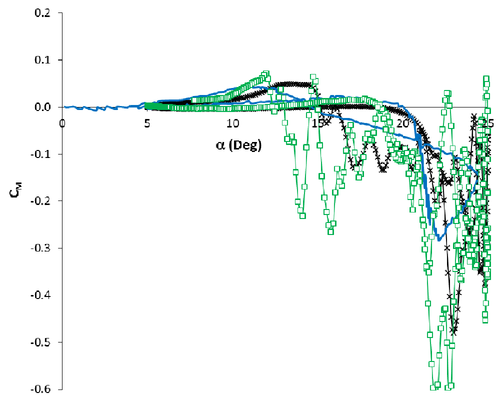

c) C_M versus α.

Fig 11: Comparison of measured [6] and computed forces and moments for the case, M= 0.09, Re_c=2.5x10^6, f=0.41 Hz, k=0.05, α=15° + 10° sin(ωt).

Here the maximum incidence of 25° is well beyond the static stall angle of ~16° for the NACA0012 at this Reynolds number. The experimental lift and pitching moment curves clearly follow the trends expected of the flow around an oscillatory pitching aerofoil with dynamic stall, with a spike in lift followed by a sharp stall, corresponding with a pitching moment divergence.

The predicted lift variations, for both turbulence model cases, correctly resolve the large lift hysteresis loop involving the lift spike due to the formation of the stall vortex at the leading edge, the subsequent large loss of lift, and the recovery to attached flow condition. The Spalart-Allmaras model, however, predicts a divergence from linear lift behavior that occurs much earlier on the upstroke than seen in the experimental data, whereas the *k-ω SST* model resolves this much better. The S-A model predicts a very early and very abrupt stall vortex formation event, with very high suction leading to over predictions in the lift peak and maximum negative pitching moment, whereas the *k-ω SST* model, again, provides a better comparison with experimental evidence. The S-A prediction captures more unsteadiness in the fully-stalled flow, and a late recovery to attached flow (linear-lift) behavior, while the *k-ω SST* model resolves the corresponding lift level, and recovery to attached flow much better.

Both turbulence models predict very similar drag characteristics, with peak drag level, at stall vortex formation, being over-predicted by ~30%.

Figure 12 presents the corresponding comparisons for the same conditions, but for the higher pitching rate of 1.22Hz, (k = 0.15). Here, the data density is less for the CFD solutions, since the time-step resolution was kept the same. Again, the *k-ω SST* model is seen to do a better job in matching the experimental characteristics than the S-A model, particularly in the post-stall period of the oscillation.

While there are clearly issues with the CFD ability to capture the fine detail of the flow evolution in these cases (and it is important to remember that there is considerable level of measurement inaccuracy inherent in any experimental data of this type), it is shown that RANS solutions can successfully resolve the principle flow events and characteristics of this complex class of unsteady flow.

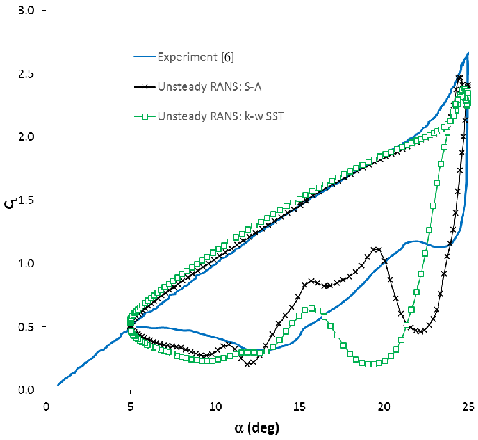

d) C_L *versus* α.

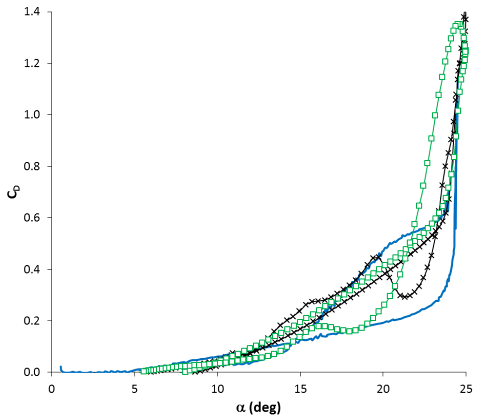

e) C_D *versus* α.

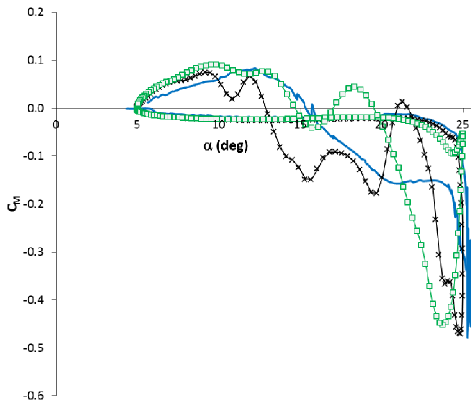

f) C_M *versus* α.

Fig 12: Comparison of measured [6] and computed forces and moments for the case, M= 0.09, Re_c*=2.5x10*^{6}*, f=1.22 Hz, k=0.15,* α*=15° + 10° sin(*ωt*).*

Figure 13 presents a sample of computed instantaneous velocity contours at certain instants during the pitch cycle for the highest pitch rate case. The CFD shows an attached flow at low α, a trailing edge separation forming and moving upstream with increasing α on the upstroke, leading edge separation and the formation of a stall vortex which rapidly convects downstream, shedding at the trailing edge around the same time as the formation of a second leading edge vortex which gets subsumed into the fully stalled upper surface flow during the downstroke prior to recovery of leading edge suction and the downstream retreat of the separation front.

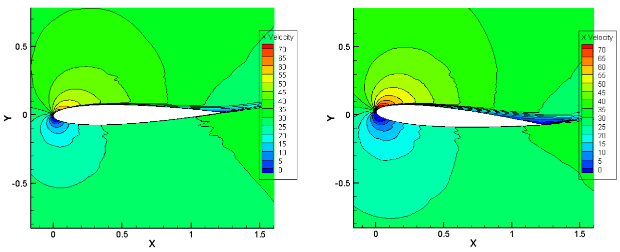

a) α =13.9 ^{o}, C_L=1.39 *b) α =19.5 ^{o}, C_L=1.80*

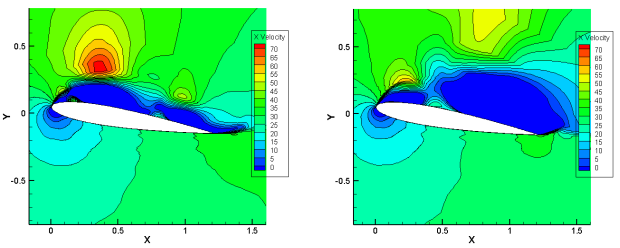

c) α =24.4 ^{o}, C_L=2.46 *d) α =25.0 ^{o}, C_L=2.41*

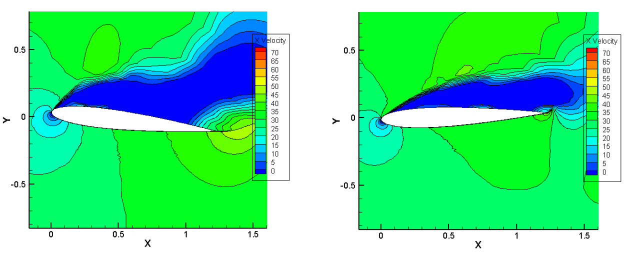

e) α =21.9 ^{o}, C_L=0.47 *f) α =13.0 ^{o}, C_L=0.35*

Fig 13: Computed velocity contours for pitching NACA 0012 aerofoil, M=0.09, Re_C =2.5 x 10^6 , α= 15 ^{o} + 10 ^{o} sin ωt, k=0.15 (Note: α is offset by 15 ^{o} so only cyclic motion is depicted).

6 Validation of the small scale test rig

With the capability of the RANS method to predict the physics of the overall flow evolution from an oscillatory pitching aerofoil, now demonstrated, the CFD method was used to validate experimental data from the new, small scale experimental test rig. Figures 13 and 14 present sample comparisons of the integrated unsteady forces (lift and drag) obtained in the experiments, with the corresponding CFD results, employing the *k*-ω SST turbulence model.

Figure 14 plots the instantaneous lift and drag comparison for a pitching rate at *k* = 0.10, and the relatively low pitch amplitude of 10°. Here, the maximum pitch angle is less than the measured static stall angle of attack (~14° in this case), and so no dynamic stall phenomena would be expected. It can be seen that both the experimental lift curve and the CFD predicted result agree very well, exibiting only a small level of hysteresis. The agreement in the drag characteristics is also relatively good.

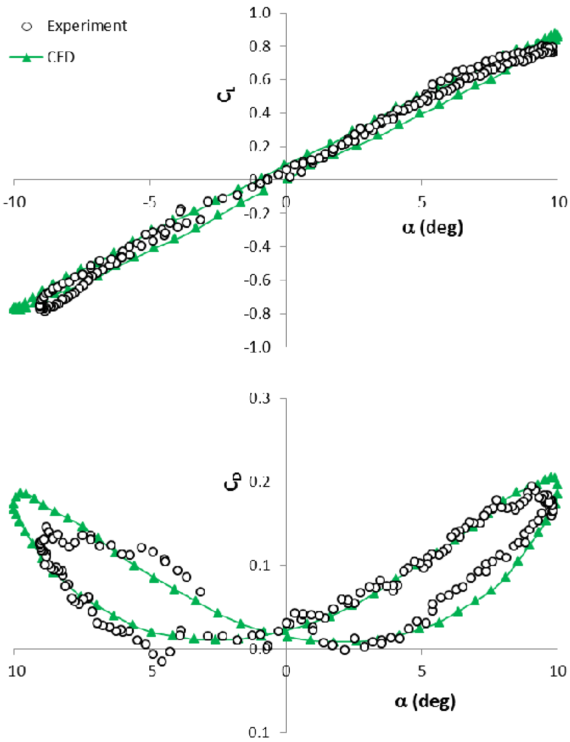

Fig 14: Variation of C_L and C_D with angle of attack for pitching NACA 0012 aerofoil, U=22m/s, Re_c = 1.48x10^5, f = 5.6Hz, k=0.1, α= 10 ^{o} sin ωt.

The corresponding comparison for the much higher pitching rate, where k = 0.33, is plotted in figure 15, where the pitch amplitude is still below the static stall condition. With a much higher pitching rate, the level of viscous hysteresis in lift and drag would be expected to be significantly greater and this is, indeed, what both the experimental measurements and the CFD solution resolve. While the agreement between the two sets of data are, again, relatively good, it is interesting to note that the experimental lift diverges from the CFD prediction with negative angle of attack. This is probably due to asymmetric flow development within the working section – something that requires investigation and, if possible, corrective action.

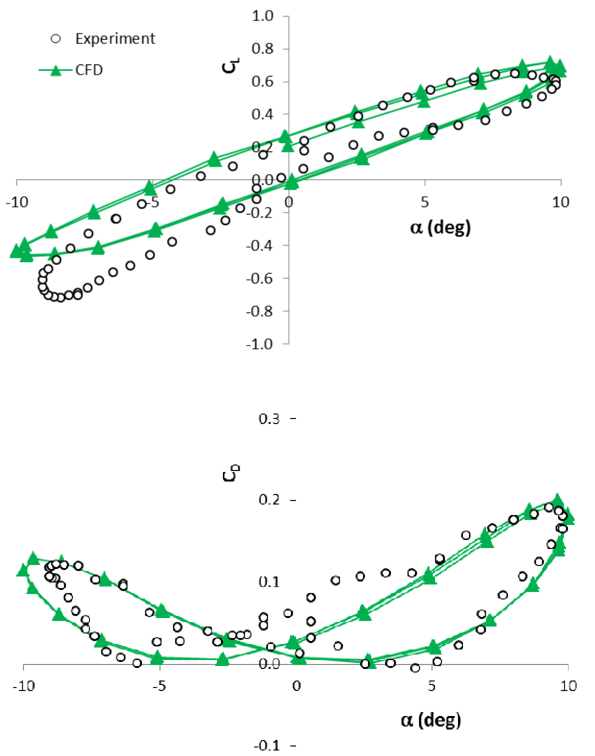

Fig 15: Variation of C_L and C_D with angle of attack for pitching NACA 0012 aerofoil, U=22m/s, $Re_c = 1.48x10^5$, f = 18.5Hz, k=0.33, $\alpha = 10^0 \sin\omega t$.

7 Conclusions

The original aim of developing the small scale oscillatory pitch and heave test rig was to enable the preliminary, comparative, testing of flow control methods to manipulate the complex unsteady flows associated with pitching aerofoils, particularly involving dynamic stall.

The results of the initial commissioning tests, reported in this paper, have shown that the rig, and the associated measurement instrumentation, should be able to resolve the effect of flow control, if that effect is relatively large.

A more focused campaign of testing is needed to further validate the experimental capability, particularly for cases with higher pitch amplitude, where strong dynamic stall phenomena will occur.

References

[1] Katzmayr, R. "Effect of Periodic Changes of Angle of Attack on Behavior of Airfoils", NACA TM 147, 1922.

[2] Reid, E. G., "Airfoil lift with changing angle of attack", NACA TN-266, 1927.

[3] Kramer, M. "Increase in the Maximum Lift of an Airfoil Due to a Sudden Increase in its Effective Angle of Attack Resulting from a Gust" NACA TM-687, 1932.

[4] Leishman, G., "*Principles of Helicopter Aerodynamics*", Cambridge University Press, 2000.

[5] Theodorsen, T. "General Theory of Aerodynamic Instability and the Mechanism of Flutter", NACA Report 496, 1935.

[6] K. W..McAlister, L. W. Carr, and W. J. McCroskey, "*Dynamic Stall Experiments on the NACA 0012 Airfoil*", NASA TP 1100. 1978.

[7] Amitay, M., Kibens, V., Parekh, D. & Glezer, A., "*The Dynamics of Flow Reattachment Over a Thick Airfoil Controlled by Synthetic Jet Actuators*", AIAA Paper 1999-10011, 1999.

[8] Woo, G. & Glezer, A., "*Transient Control of Separating Flows over a Dynamically-Pitching Airfoil*", AIAA Paper 2010-861, 2010.

[9] Visbal, M. R., "Control of Dynamic Stall on a Pitching Airfoil Using High Frequency Actuation", AIAA Paper 2015-1267, 2015.

[10] Pope, A. & Harper, J. J., "*Low Speed Wind Tunnel Testing*", John Wiley and Sons, New York, 1966.

[11] J. A. Ekaterinaris and M. F. Platzer, "*Computational Prediction of Airfoil Dynamic Stall*", *Prog. Aerospace Sci.*, vol. 33, no. 11–12, pp. 759–846, 1998.

[12] Ke., J., & Edwards, J. R. " RANS and Hybrid LES/RANS Simulations of Flow over a Pitching NACA 0012 Airfoil", AIAA Paper 2015-0311, 2015.

Contact Author Email Address

For information on this work contact either:
simon.prince@cranfield.ac.uk or
J.C.Holt@cranfield.ac.uk.

Copyright Statement